



A Novel Magnetic Flux Leakage Testing Method Based on AC and DC Composite Magnetization

Rongbiao Wang¹ · Yihua Kang¹ · Jian Tang¹ · Bo Feng¹ · Yongle Deng¹

Received: 27 June 2020 / Accepted: 31 October 2020 / Published online: 9 November 2020
© Springer Science+Business Media, LLC, part of Springer Nature 2020

Abstract

The flexible printed coil array (FPC) is employed extensively because of its flexibility in non-destructive testing (NDT). To make the inductive coil detect both external and internal defects under static conditions in magnetic flux leakage testing (MFL), this paper proposes a method based on the AC and DC composite magnetization. The AC magnetization changes the magnetic field strength in the vicinity of external defects. The DC magnetization makes the defects generate static leakage magnetic field. The permeability in the skin layer is also altered by the AC magnetization which affects the transmission of leakage magnetic field caused by internal defects. Therefore, external and internal defects can generate a time-varying leakage magnetic field. Simulations and experiments are carried out to validate the feasibility of this method. The results indicate that the method based on the AC and DC composite magnetization can be applied to detect both external and internal defects.

Keywords Composite magnetization · Magnetic shielding · MFL · Internal defects · Permeability

1 Introduction

The flexible sensor array is widely applied in non-destructive testing (NDT) [1], such as the flexible ultrasonic array probe [2–4] in ultrasonic testing (UT) and the flexible printed coil array (FPC) probe [5–8] based on printed circuit board (PCB) in eddy current testing (ECT). With the FPC, a certain area can be detected without scanning. Besides, the specimen with complex contours such as the pipe bend and the welded seam can be inspected because the shape of FPC can be changed to suit the contour. Because of its advantage, it is gradually used in the direct current magnetic flux leakage (DC-MFL) testing [9] which is applied widely in the detection of ferromagnetic materials. However, the FPC can only measure the change of the magnetic field rather than the absolute value of the leakage magnetic field [10]. Therefore, the FPC can be applied at high speed. While under the condition that the high detection speed cannot be realized, such as the detection of pipe bends and in-service inspection, the FPC is unable to detect the static leakage magnetic field.

In order to detect the defect with coils statically, the alternating current magnetic flux leakage (AC-MFL) technique can be adopted, which generates a time-varying magnetic field [11, 12]. However, due to the skin effect, only surface or near-surface defects can be detected [13]. To improve the penetration depth of AC-MFL, Tsukada et al. [14] used the excitation current with extremely low frequencies. The back-side pitting of a 10 mm thickness plate can be detected by analyzing the magnetic field component parallel to the inducing magnetic field. Song et al. [15] analyzed the phase change in the detected signal by low-frequency magnetic flux leakage (LFMFL) method to detect the internal defect. Although the skin depth can be increased by reducing AC frequency, only defects in a limited buried depth can be detected. Moreover, the sensitivity of induction coils will decrease with reducing frequency [16]. To achieve the detection of defects with deeper depth, Sophian et al. proposed pulsed magnetic flux leakage (PMFL) techniques [17]. The stepped excitation was applied as the magnetizing current. This method has the advantage of detecting deeper subsurface defects, locating and sizing defects. Wilson et al. further complemented the PMFL by combing pulsed magnetic reluctance (PMR) technique, which improved sub-surface defects characterization capabilities [18]. And Wilson et al. used feature extraction and integration of PMFL data to enhance defect characteriza-

✉ Yihua Kang
yihuakang@hust.edu.cn

¹ State Key Lab of Digital Manufacturing Equipment & Technology, Huazhong University of Science and Technology, Wuhan, China

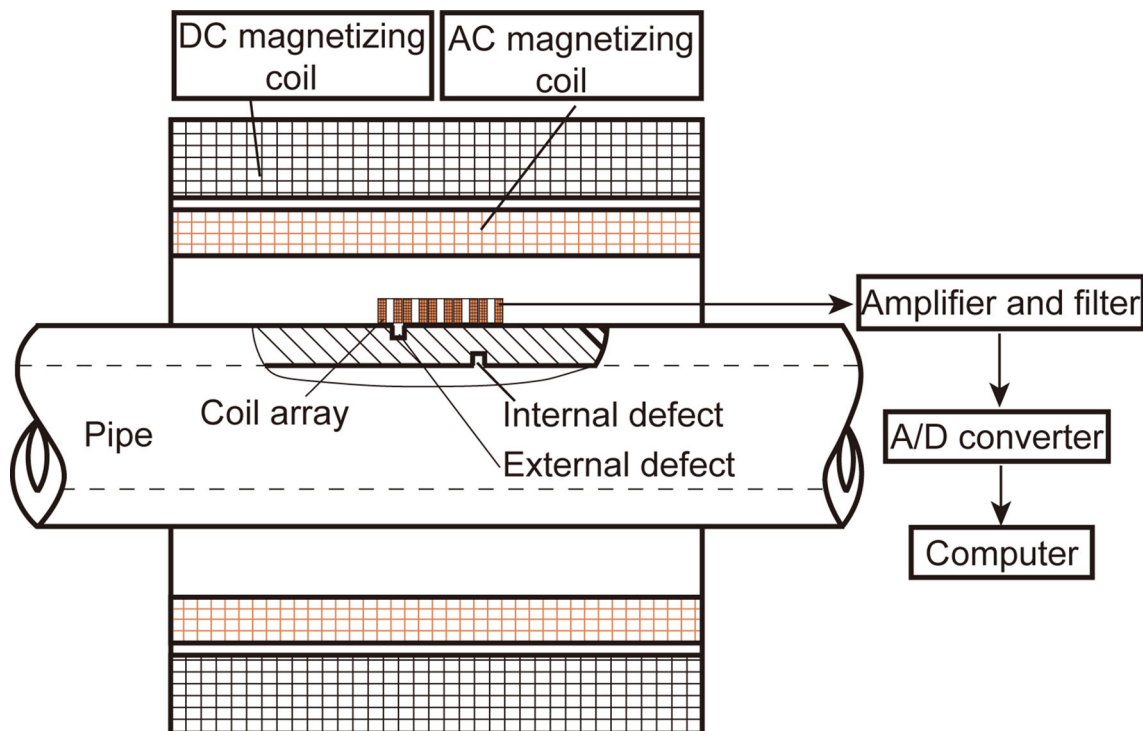


Fig. 1 The schematic diagram of the method

tion capabilities [19]. Wang et al. applied sensor array based PMFL technology to detect rail cracks [20].

The penetration depth of DC-MFL testing is more than 15 mm [21], and the ferromagnetic materials with high permeability surrounding the subsurface defects could shield the MFL [22, 23]. To extend the depth of the defects that can be detected by the static induction coil, this paper combines the advantages of deep penetration depth of DC-MFL and the characteristic that the subsurface defect signal can be affected by the permeability surrounding it. A method based on the combination of AC and DC magnetization is proposed. The DC magnetization can penetrate deeper than AC magnetization. By the DC magnetization, the internal defect generates a DC leakage magnetic field. The AC magnetization changes the permeability of the skin layer which influences the static leakage magnetic field caused by the internal defects. In addition, the change of the magnetic field strength in the skin layer changes the leakage magnetic field of the external surface defect. This makes the leakage magnetic field of both internal and external defects change with time, and they can be captured by static induction coils. In this paper, the proposed method will be introduced in detail with the steel pipe as the detection object.

2 Principle

The main configuration of the proposed method is displayed in Fig. 1. Under the magnetization of the DC magnetizing coil in Fig. 1, the steel pipe is magnetized to the near-saturated state corresponding to the point a on the B-H curve in Fig. 2a. Then, the AC magnetizing coil superimposes a coaxial alternating magnetic field with strength H_{ac} as shown in Fig. 2c. It will concentrate on the skin layer because of the eddy current effect as displayed in Fig. 3. Therefore, the external defect of the pipe is subject to a superimposed magnetization, which continuously changes with time in an AC magnetization cycle. The process of the superimposed magnetization is shown in Fig. 2b by the black line. Because of the change of the magnetic field, the external defect generates a time-varying magnetic leakage field.

For the internal defect, its leakage magnetic field transmits through the pipe wall and then reaches the external surface. The leakage magnetic field is affected by the permeability of the ferromagnetic materials. The permeability of the skin layer changes with the AC magnetization as shown in Fig. 2b by the blue line, so the leakage magnetic field is changed by the permeability of the skin layer when it passes through the skin layer of the pipe. To make the leakage magnetic field

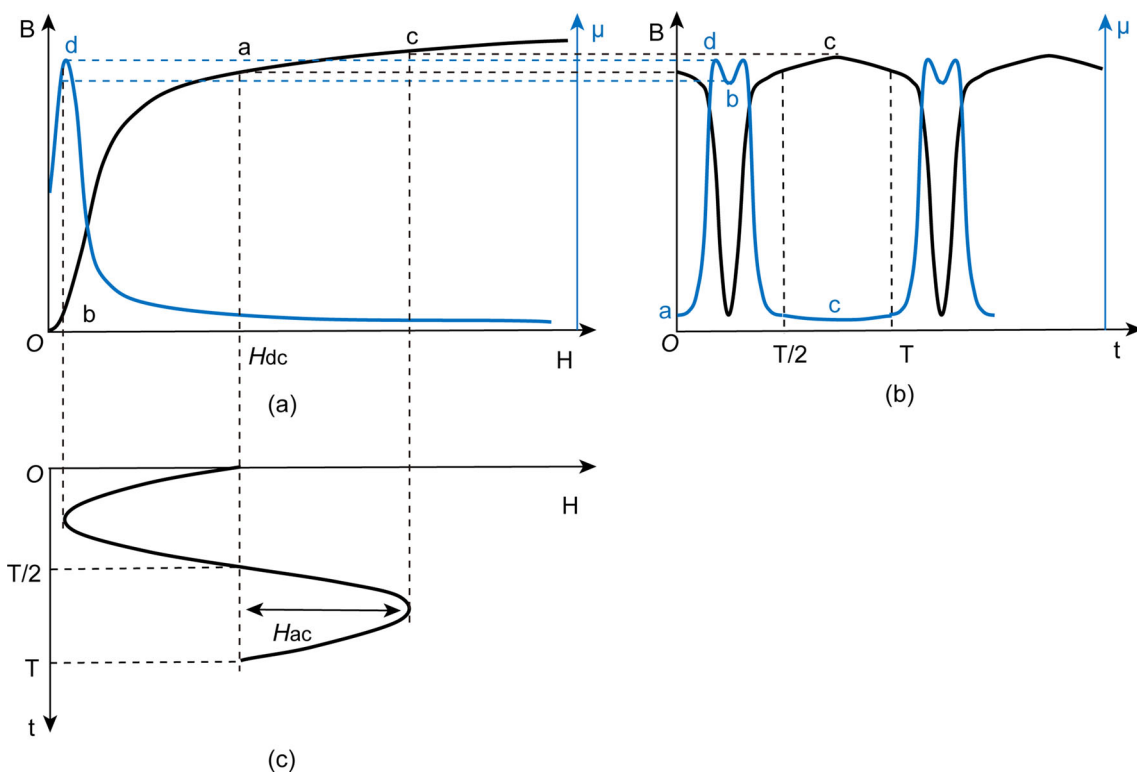


Fig. 2 The magnetizing process

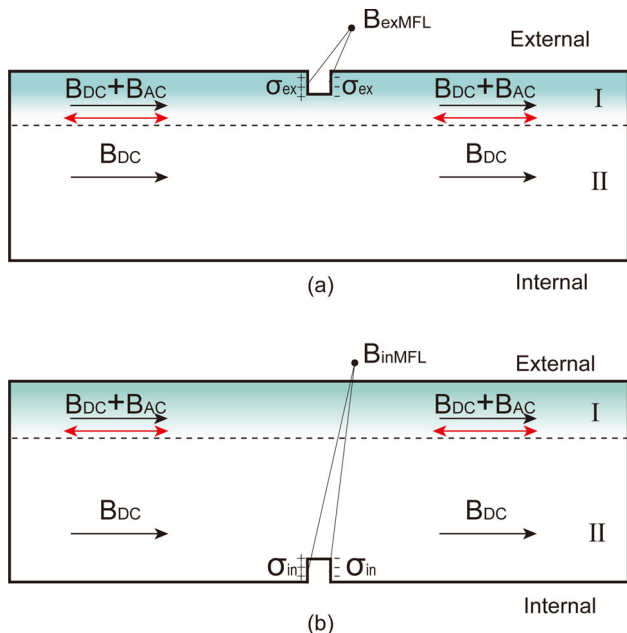


Fig. 3 The schematic diagram of the magnetic field distribution

above the surface change, the process is divided into two parts as follows.

(1) The internal leakage magnetic field is prevented from diffusing into the air. The magnetic permeability in the sur-

face layer of the steel pipe (area I in Fig. 3b) should be as large as possible to form a shielding layer due to the shielding effect of the high permeability material. Therefore, when the AC magnetic field and the DC magnetic field are in opposite directions, the magnetic permeability of the surface layer reaches the maximum value. The leakage magnetic field is prevented from diffusion due to the shielding effect. The magnetizing process is shown in Fig. 2a, b. The magnetization state of the skin layer on the B-H curve changes from the point a to the point b, and the magnetic permeability μ increases accordingly. Therefore, the leakage magnetic field in the air gradually decreases with time.

(2) The diffusion of the internal leakage magnetic field into the air is promoted. The magnetic permeability in the outer layer of the steel pipe (area I in Fig. 3b) should be as small as possible. When the AC magnetic field and the DC magnetic field are in the same direction, the permeability of the surface layer reaches the minimum, which promotes the diffusion of the leakage magnetic field. On the B-H curve, as the magnetization state in the skin layer of the steel pipe changes from the point a to the point c, the magnetic permeability μ decreases, and the leakage magnetic field in the air gradually increases.

Therefore, during a cycle of AC magnetization, the leakage magnetic field generated by the internal defects diffuses into the air periodically. Both the internal and external defects

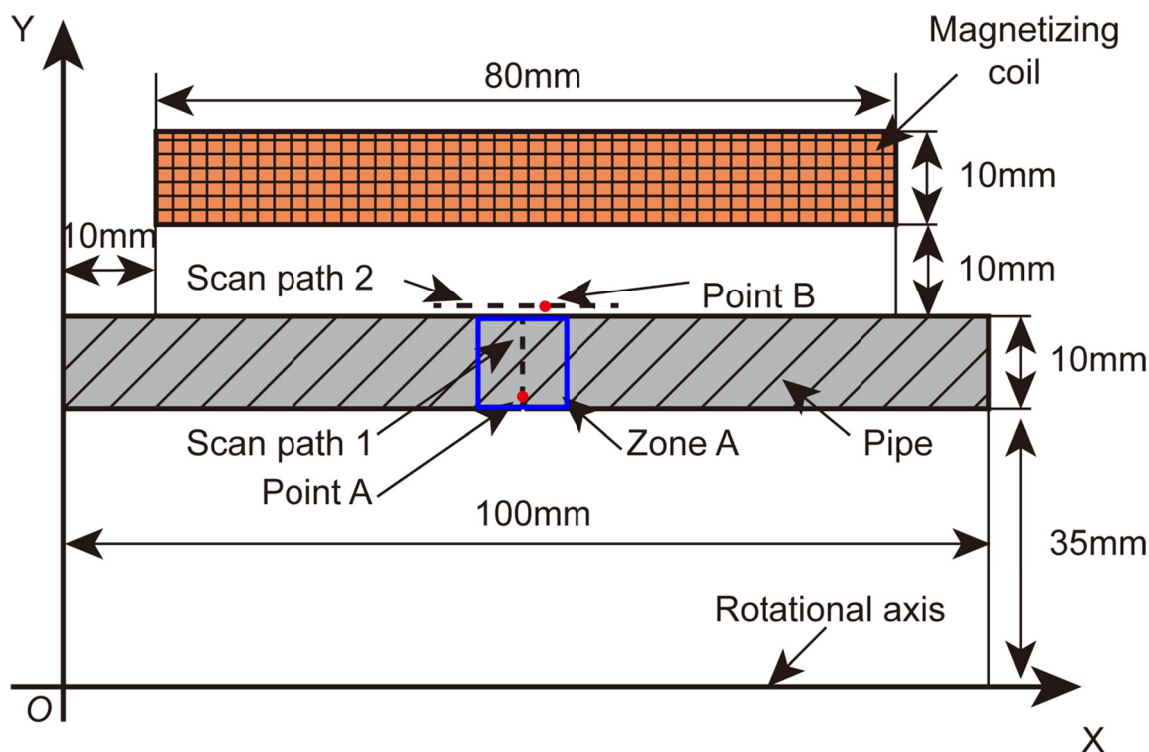


Fig. 4 The simulation model without defects

produce a time-varying leakage magnetic field, and they can be detected by static coils.

It should be noted that magnetic hysteresis exists in the magnetizing process. To make the illustrations in Fig. 2 clear, the hysteresis loop is not shown.

3 Simulation Analysis

A two-dimensional rotational axisymmetric simulation model was established in the JMAG-Designer18.1 software. The model is mainly composed of a steel pipe and a magnetizing coil. The material of the steel pipe was set to be S45C, and its isotropic non-linear magnetic characteristics were realized by setting a B-H curve to the material. The magnetizing coil with 2000 turns provided superimposed magnetization for the steel pipe. Scan path 1 starts from the point (50, 35) to the point (50, 45), and scan path 2 starts from the point (40, 45.5) to the point (60, 45.5). The geometry of the entire model is shown in Fig. 4.

The transient analysis was applied to simulate the magnetic field distribution and permeability distribution of the steel tube under superimposed magnetization. Compared with the stepped excitation in PMFL method and the sinusoidal excitation in AC-MFL method, the magnetizing current was superimposed by AC magnetizing current (with an amplitude of 1.5 A and a frequency of 200 Hz) and DC mag-

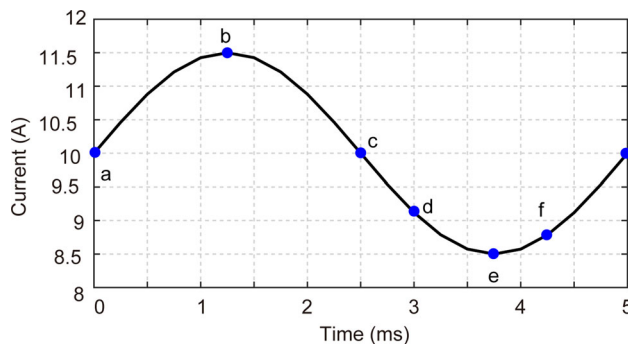


Fig. 5 The magnetizing current

netizing current (with an amplitude of 10 A). One full cycle of the magnetizing current is shown in Fig. 5 and it is divided into 20 simulation steps. Points a-f represent some simulation steps. Because there is a coil in the excitation circuit, so the circuit is not a pure resistive circuit, which includes an inductance. The steel pipe also contributes mutual inductance to the circuit. When the RL circuit is under an AC excitation, it requires several cycles for the current to reach a stable state in the coil. The following simulation results were all extracted after the calculation results were stable.

As a result of the skin effect, the change of the magnetic flux density is different in the thickness direction within an excitation cycle. Along the scan path 1 in Fig. 4, the maximum (B_{acmax}) and minimum (B_{acmin}) values of the magnetic

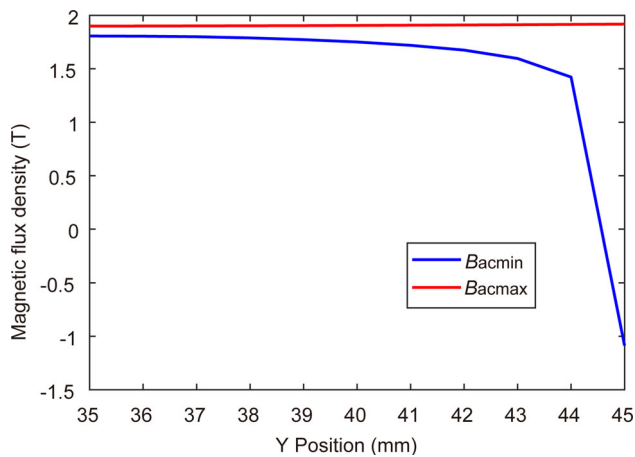


Fig. 6 The distribution of magnetic flux density along the scan path 1

flux density component along the X direction within one excitation cycle were extracted and their distribution is plotted in Fig. 6. The X axis direction represents the pipe's thickness direction. The red line shows that the change of B_{acmax} in the pipe's thickness direction is small while the change of B_{acmin} is great as shown by the blue line. The difference of the red line and the blue line represents the change of the magnetic flux density within an excitation cycle. From Fig. 6, it can be seen that the magnetic flux density on the surface of the steel pipe changes greatly within an excitation cycle. The change decreases sharply along the scan path 1 and it is small on the inner wall.

As analyzed in the principle, the magnetic permeability also influences the MFL apart from the magnetic flux density in the pipe. At different steps in a cycle, the relative permeability distribution in zone A on the cross-section of the steel pipe in Fig. 4 is shown in Fig. 7. The six figures correspond to the six steps in Fig. 5. It can be seen that the steel pipe is magnetized to the near-saturated state in the positive half cycle (points a, b, and c) because the relative permeability is small. Therefore, when the magnetizing current continues to increase, the change of the relative permeability of the steel pipe is small. However, when the direction of AC magnetization is opposite to that of DC magnetization in the negative half cycle (points d, e, and f), the surface magnetic field strength decreases. From the B-H curve in Fig. 2, it can be known that the decrease of the surface magnetic field strength will cause the increase of the relative permeability when the specimen is already in the near-saturated state. Besides, the magnetic flux density can reach to 0 T in the skin layer as indicated by Fig. 6. Therefore, the permeability of the surface layer changes greatly. From Fig. 7a–c, it can be seen that the relative permeability is big in the skin layer which is consistent with the previous theoretical analysis.

After analyzing the internal magnetic flux density distribution and the magnetic permeability distribution of the steel

pipe without defects, with the same simulation parameters, simulation models with the internal and external defects were established as displayed in Fig. 8a, b. The dimensions of the defects on the inner and outer surfaces are 1 mm in width and 1 mm in depth.

Firstly, the external surface defect signal is analyzed. Along the scan path 3 in Fig. 8, the normal component of the magnetic flux density B_y of 10 simulation steps were extracted, and the corresponding background magnetic flux density along the scan path 2 in Fig. 4 were subtracted to obtain the MFL distribution at different steps. The results are plotted in Fig. 9a. Because the coil is placed at a certain point to detect the defects in practical applications, the change of MFL with time is analyzed at a specific point. The normal component of the magnetic flux density at the point C (50.5, 45.5) in Fig. 8a was subtracted from the background magnetic flux density at the point B (50.5, 45.5) in Fig. 4 to obtain the change of the leakage magnetic field with time caused by the defect. The results are plotted in Fig. 9b. Similarly, the calculation results of the internal defects are plotted in Fig. 10a, b.

Figure 9 shows that the leakage magnetic field of the external defect changes greatly because of the change of the magnetic flux density in the skin layer. For the internal defects, the leakage magnetic field still changes from the maximum to near zero as shown by Fig. 10. When AC magnetization is in the same direction as DC magnetization, Fig. 10b shows that the change of the leakage magnetic field is relatively small. On one hand, the skin effect causes that the change of the magnetic flux density in the vicinity of the internal defect is small as indicated by Fig. 6. On the other hand, the relative permeability of the skin layer is not greatly reduced when the pipe is in the near-saturated state. When AC magnetization and DC magnetization are in opposite directions, the minimum value of the leakage magnetic field is close to 0 as displayed by Fig. 10b because of the increase of the relative permeability in the skin layer as shown in Fig. 7d–f. The high relative permeability layer shields the leakage magnetic field.

It can be seen from Fig. 6 that although the magnetic field change on the inner surface is small, it can still cause the change of MFL. In order to further verify the shielding effect of the magnetic permeability on the leakage magnetic field of the internal defect, the maximum value B_{max} and the minimum value B_{min} of the magnetic flux density were extracted at the point A (50, 35.5) (the middle of the internal defect) within one excitation cycle in the simulation model shown in Fig. 4. Then the simulation model shown in Fig. 4 was applied for DC-MFL simulation. Except for the magnetizing current, other parameters were not changed. By continuously changing the magnitude of the DC magnetizing current, the magnetic flux density at the point C reached the maximum value B_{max} and the minimum value B_{min} , respectively.

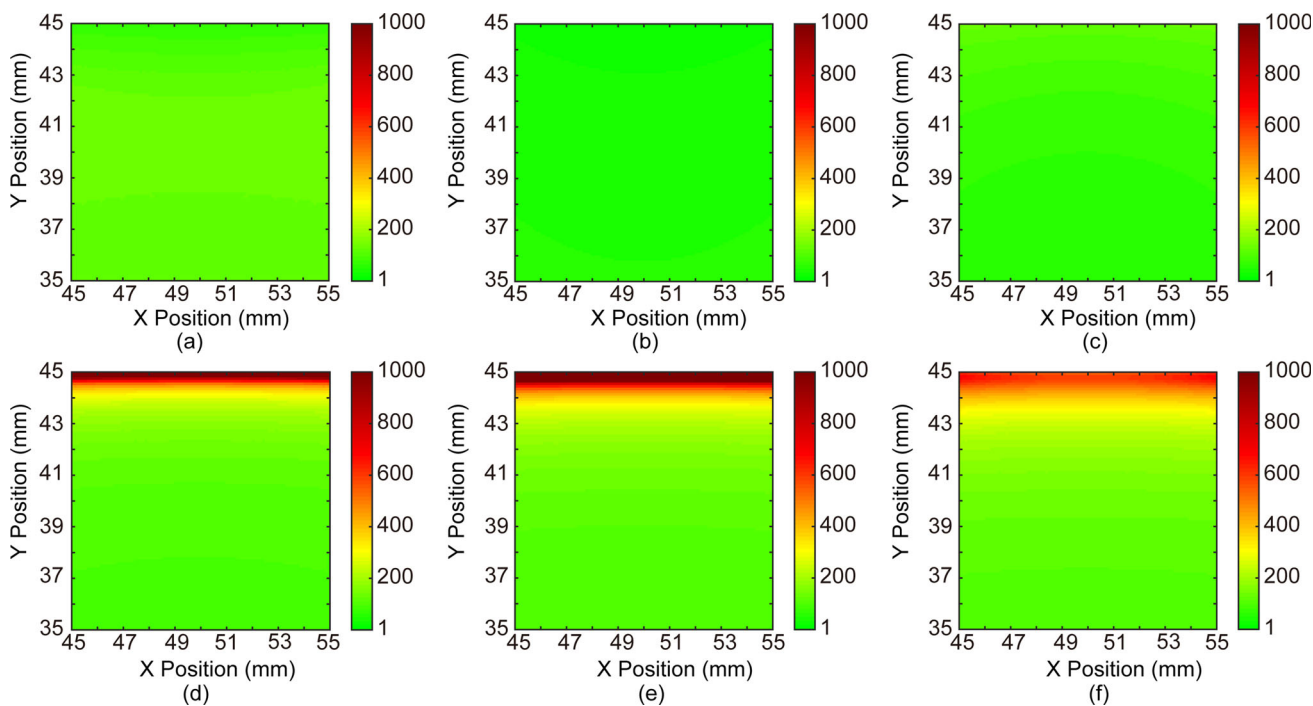


Fig. 7 The distribution of the permeability

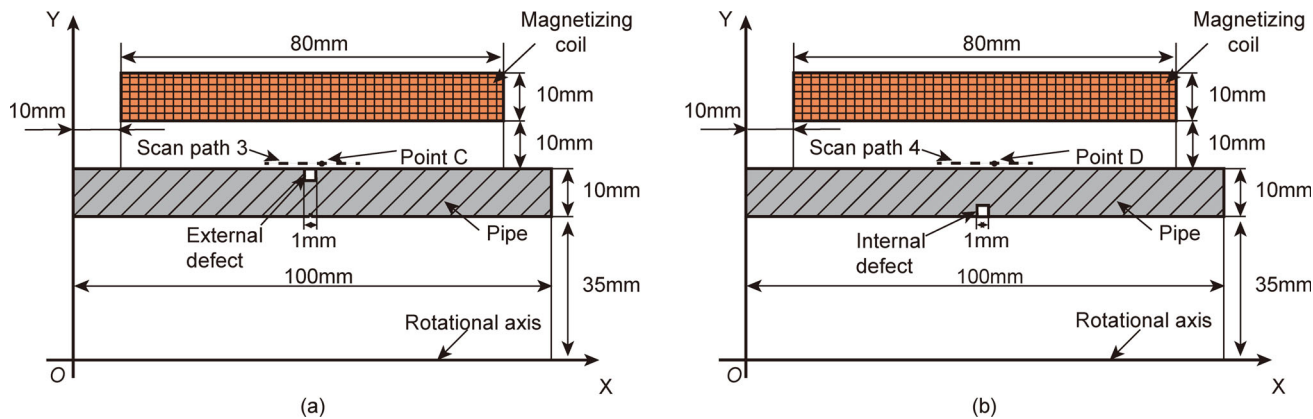


Fig. 8 The simulation model with defects

The corresponding magnetizing currents I_{dcmax} and I_{dcmin} were recorded, and then DC magnetization on the simulation model in Fig. 8b was performed. The magnetizing currents were respectively set to I_{dcmax} and I_{dcmin} , and the MFL distributions corresponding to the two magnetizing currents were obtained along the scan path 4. After the background magnetic flux density was subtracted, the results are plotted in Fig. 11.

It can be seen that the amplitude of the leakage magnetic field also changes to a certain extent under the effect of the magnetic flux density change on the inner wall. The change of leakage magnetic field caused by the change of inner wall magnetic flux density is 14 mT, while the change of leakage

magnetic field caused by the skin layer permeability shielding can reach 32 mT as shown in Fig. 11.

4 Experiments

In this section, an experimental system was built to verify this method as shown in Fig. 12. The specimen is a 45# steel pipe with a diameter of 89 mm and a wall thickness of 10 mm as shown in Fig. 13. The inner and outer walls of the steel pipe were respectively etched with notches (0.5 mm in width and different depths (1.0 mm, 1.5 mm, 2.0 mm, 2.5 mm, and 3 mm)) by electric discharge machining (EDM). The axial magnetization was generated by the DC magnetizing

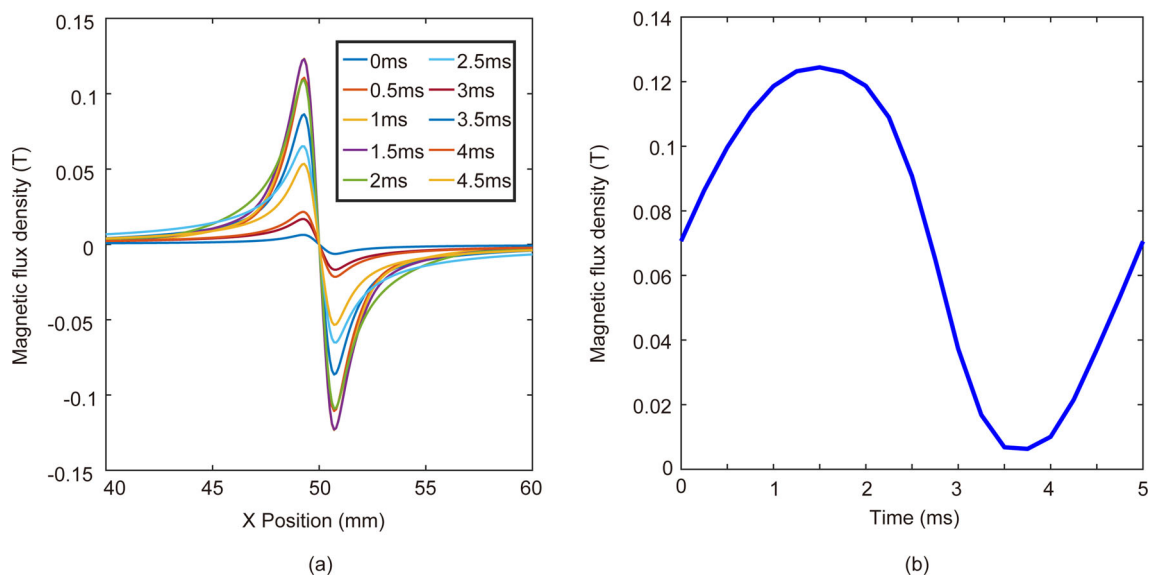


Fig. 9 The MFL distribution of the external defect

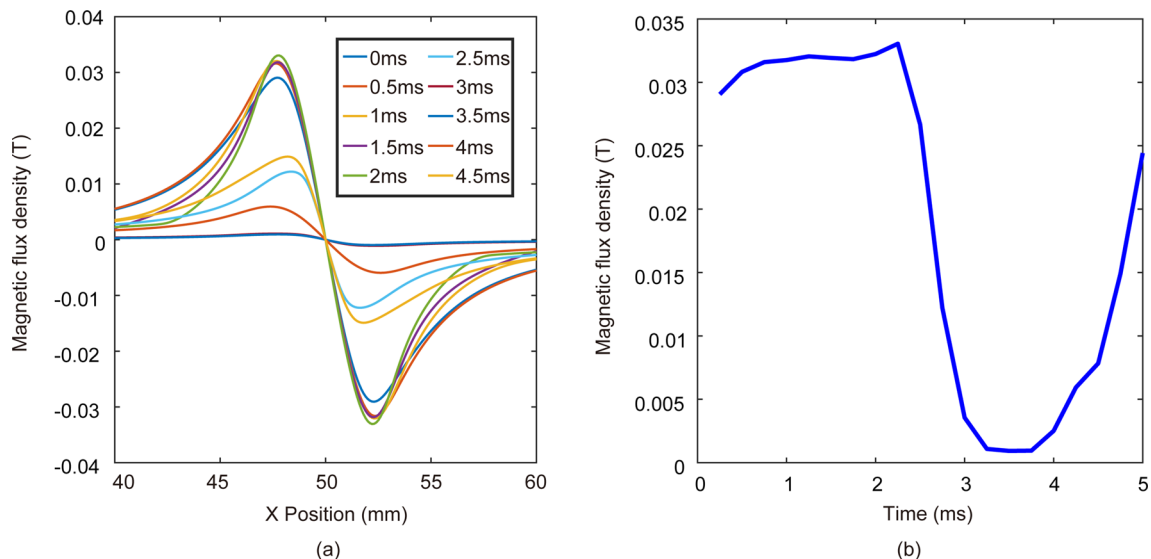


Fig. 10 The MFL distribution of the internal defect

coil with 3600 turns, which was powered by a DC magnetizing power source. The AC magnetizing coil with 2000 turns and powered by an AC magnetizing power source with a frequency of 200 Hz provided AC axial magnetization. The outer and inner diameters of the pick-up coil with 300 turns are 4 mm and 3 mm respectively. The output voltage of the coil was processed by an amplifier with a gain of 1000 and a low-pass filter with a cutoff frequency of 300 Hz. The experimental data was displayed on the computer software after A/D conversion with the acquisition frequency of 2 kHz.

Firstly, a pick-up coil was placed on the outer wall below which there is an internal defect with a depth of 1.0 mm. The distribution of the normal component of the MFL is

anti-symmetrical about the middle of the defect as illustrated in Fig. 9a and Fig. 10a. If the pick-up coil is placed right above the defect, the magnetic flux caused by the defect is zero. Therefore, the axis of the pick-up coil was slightly deviated from the middle of the defect. As a reference, another pick-up coil was placed on the outer wall where there are no cracks on both the inner and outer walls. The frequency of the AC magnetizing current was 200 Hz and the current was 1.5 A. The DC magnetizing current was gradually increased from 0 to 10 A. The peak values of the signal from the coil above the internal defect were collected and then subtracted the peak values of the reference coil signal. The change of the volt-

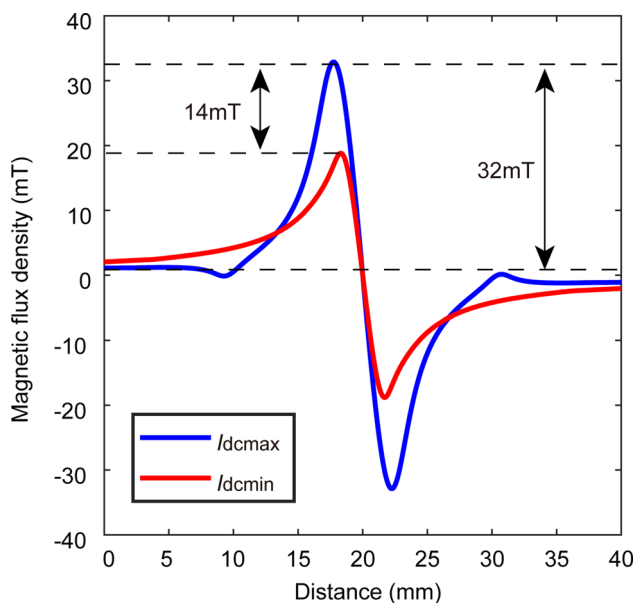


Fig. 11 The MFL distribution of the internal defect with different DC magnetizing currents

age difference with DC magnetizing current is shown in Fig. 14.

Then, the DC magnetizing current was adjusted to 6A corresponding to the current value where the voltage difference was the largest as shown in Fig. 14. The detection coil was

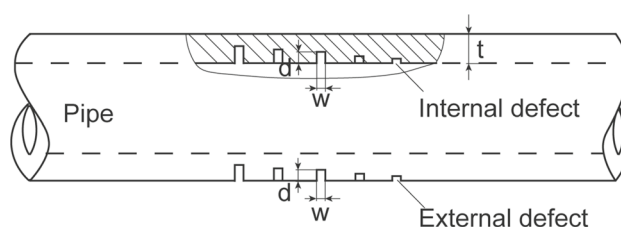


Fig. 13 The specimen

placed on other defects, respectively. The reference coil was placed in the defect-free region. The output voltage signals of the coils are shown in Fig. 15 when the detection coil was placed above the internal defect with a depth of 1 mm. Afterwards, the dependence of the voltage difference on the depth of defects were studied. The voltage difference is plotted in Fig. 16 as a function of the depth of the external and internal defects respectively. The error bars represent the mean and standard deviations of the signals measured multiple times with the same experiment parameters repeatedly.

Figure 14 shows that when only the AC magnetization is applied, due to the limitation of the skin effect, the pick-up coil cannot detect the internal defect. With the increase of the DC magnetizing current, the DC magnetization strength on the inner wall increases, which results in the increase of DC-MFL caused by the internal defect. Under the effect of the permeability of skin layer, the amplitude of the AC-

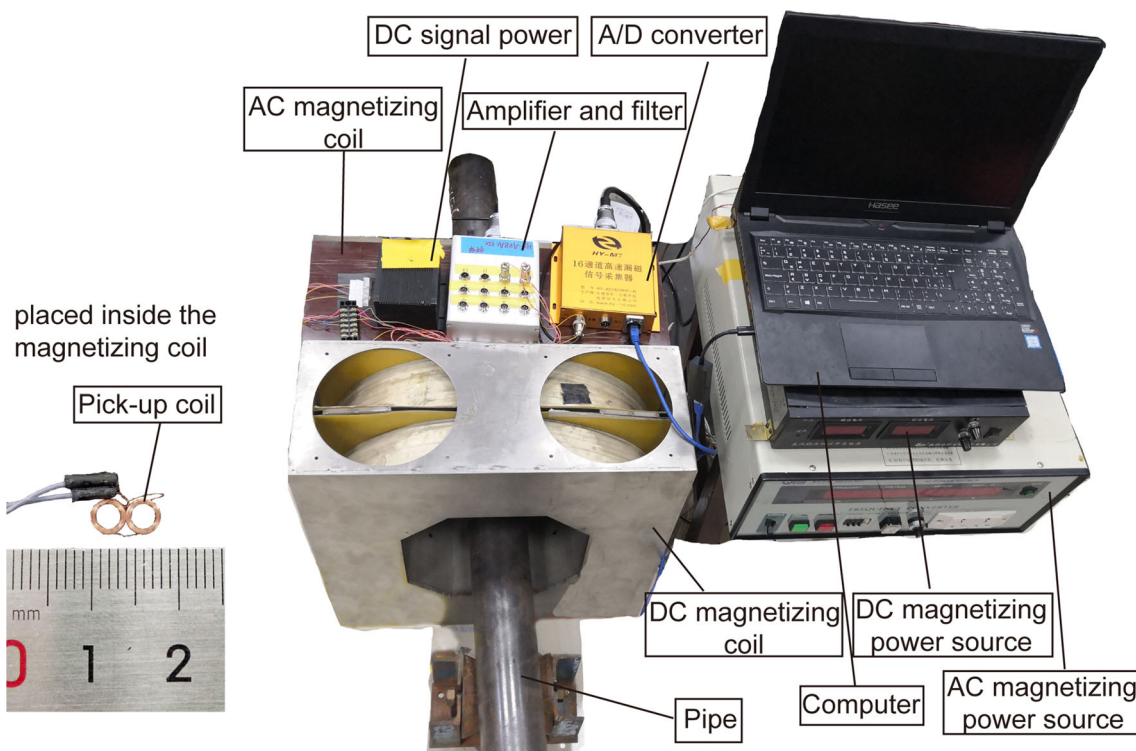


Fig. 12 Experimental systems

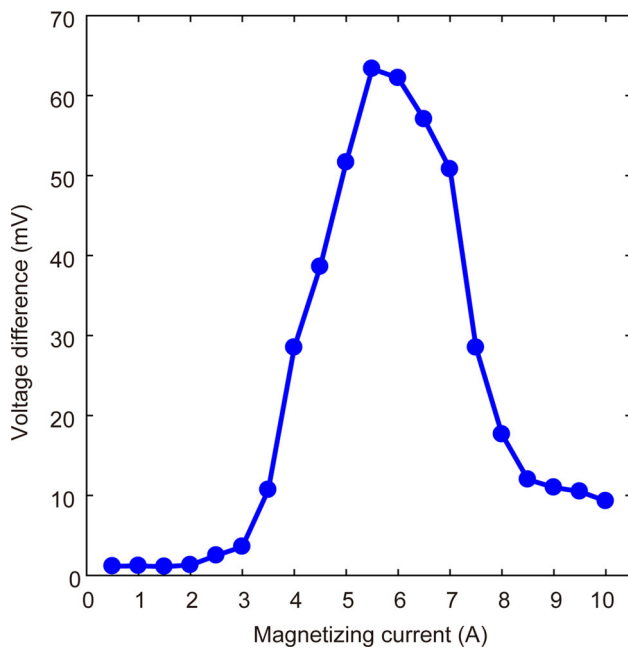


Fig. 14 Dependence of the voltage difference on the DC magnetizing current

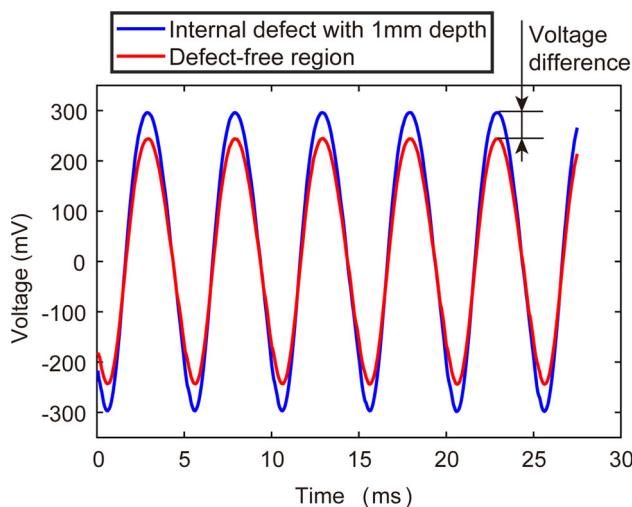


Fig. 15 The voltage of the internal defect and defect-free region

MFL above the pipe surface increases, so the peak value of the detection signal above the surface increases accordingly. When the DC magnetizing current is further increased, the DC magnetizing point on the B-H curve shifts to the right-hand side as displayed in Fig. 2a while the alternating magnetic field strength H_{ac} is not changed. Therefore, during an AC magnetization cycle, the maximum value of the surface magnetic permeability gradually decreases, weakening the shielding effect on the leakage magnetic field caused by the internal defects. As a result, the variation of the AC-MFL is reduced which causes the decrease of voltage difference value.

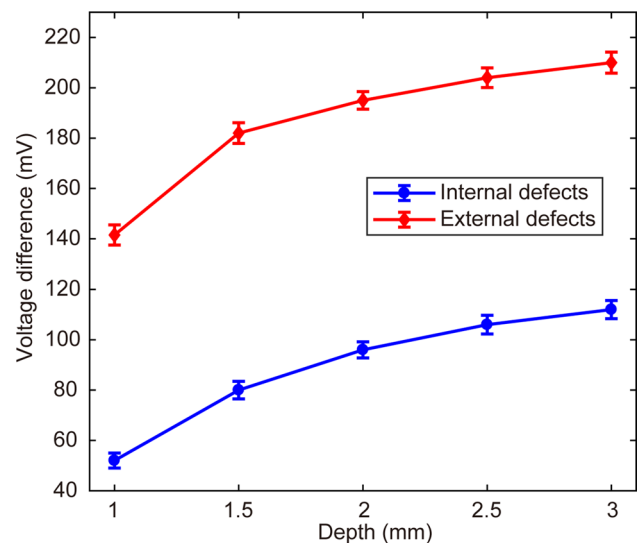


Fig. 16 The voltage difference versus depths

The experimental results in Figs. 15 and 16 show that even if the coil is stationary, it can still detect the internal and external defects, and the voltage difference gradually becomes larger as the defect depth increases.

5 Discussion and Conclusions

Conventional DC-MFL obtains the induction signal and its spatial magnetic field distribution through the probe movement. The proposed method can use the induction coil to detect internal and external defects of ferromagnetic materials under static conditions. (1). Induction coils measure the gradient of the magnetic field while sensors such as Hall probes that measure the absolute value of the magnetic field, which are easy to saturate under strong background magnetic fields [24]. (2). Besides, coils are cheap and robust in real industrial applications. And the FPC can fit on complex contours. Therefore, the detection and in-service monitoring of both external and internal defects in ferromagnetic materials can be realized by induction coils statically by this method. (3). Furthermore, the signal generating mechanism of external and internal defects is different. The leakage magnetic field of external defects is subject to the composite magnetization as shown by Fig. 3. If the B_{AC} is strong enough, the direction of the magnetization will reverse. Therefore, the direction of the leakage magnetic field generated by the external defect will change subsequently. However, for the internal defect, its DC leakage magnetic field is caused by the B_{DC} . As a result of skin effect, the change of B_{AC} of on the inner surface of the pipe is small. And the change of B_{AC} on the outer surface only changes the permeability which will not change the direction of the leakage magnetic field. Thus, the

direction of the leakage magnetic field will keep unchanged. Consequently, the distinction between internal and external defects could possibly be made based on the direction of the leakage magnetic field when the B_{AC} is properly set.

Many scholars have studied the combination of AC magnetization and DC magnetization. Under different forms of AC magnetization, the detection mechanism is different. It is common to apply a DC magnetizer in eddy current testing [25, 26]. Compared with the DC magnetic field generated by the magnetizer, the AC field intensity generated by the excitation coil is low and its frequency is high (above 10 kHz). In a magnetically saturated state, both external and internal defects can be detected. The reason is that the eddy current coil detects the magnetic permeability disturbance in the surface caused by the leakage magnetic field from internal defects. Kang et al. [27, 28] systematically studied the generation mechanism of the internal defect signal. Gotoh et al. [29, 30] superimposed weak co-directional AC magnetization on the basis of DC magnetization. The principle is that under this DC magnetization, the magnetic field strength above the internal defect increases, and the differential permeability changes under the weak AC magnetization which is different from the defect-free region. Lou et al. [31] combined an AC magnetizing coil (with the frequency of 20–50 Hz) with a DC magnetizing coil to increase the detection depth because the DC magnetization reduces the relative permeability and increases the skin depth. Because the mechanism is still based on the change of magnetic flux density on the inner wall, its detection depth is still limited by the skin effect.

The amplitude and frequency of the AC magnetic field applied in this paper are different from the above-mentioned researches. The AC magnetization is strong, which makes the magnetic field strength in the skin layer change as much as possible when the AC magnetizing current is working in a negative half cycle. Thus, the magnetic permeability in the skin layer is large which can shield the leakage magnetic field from internal defects. In this state, the signal generation mechanism of external defects is the principle of AC-MFL. The mechanism of the alternating magnetic flux leakage signal of internal defects is the shielding of MFL signals by the skin layer permeability of the steel pipe, so the detection depth is not affected by the skin depth. Compared with the method proposed by Kang et al. [27, 28] and Gotoh et al. [29, 30], the interference between excitation coils is ignored in this paper because there is only one AC magnetizing coil. Compared with PMFL [17], this method utilized the change of magnetic flux density and permeability to detect external and internal defects with static coils, respectively, while surface defects and internal defects detection is achieved by high and low frequency excitation components by PMFL method separately [32]. Because the excitation in this paper is a single-frequency sinusoidal signal, the signal processing

circuit is relatively simple in this paper compared with the PMFL method.

Since the induction coil is more sensitive to high-frequency signals, this paper studies an AC magnetization frequency of 200 Hz. However, a higher AC frequency means that the surface permeability shielding layer becomes shallower, and the shielding effect of the MFL signal needs to be further studied. In addition, this paper only uses the steel pipe to do a preliminary study, and experiments on the pipe elbow need to be conducted in further researches.

Acknowledgements This paper is financially supported by the National Natural Science Foundation of China (NNSFC) [51875226], the Launch fund of Huazhong University of Science and Technology (03), and Grant No.2017YFB0103903.

References

1. Tse, P., Fang, Z., Ng, K.: Novel design of a smart and harmonized flexible printed coil sensor to enhance the ability to detect defects in pipes. *NDT E Int.* **103**, 48–61 (2019). <https://doi.org/10.1016/j.ndteint.2019.02.003>
2. Hunter, A.J., Drinkwater, B.W., Wilcox, P.D.: Autofocusing ultrasonic imagery for non-destructive testing and evaluation of specimens with complicated geometries. *NDT E Int.* **43**, 78–85 (2010). <https://doi.org/10.1016/j.ndteint.2009.09.001>
3. Kobayashi, M., Jen, C.-K., Bussiere, J., Wu, K.-T.: High-temperature integrated and flexible ultrasonic transducers for nondestructive testing. *NDT E Int.* **42**, 157–161 (2009). <https://doi.org/10.1016/j.ndteint.2008.11.003>
4. Nakahata, K., Tokumasu, S., Sakai, A., Iwata, Y., Ohira, K., Ogura, Y.: Ultrasonic imaging using signal post-processing for a flexible array transducer. *NDT E Int.* **82**, 13–25 (2016). <https://doi.org/10.1016/j.ndteint.2016.04.002>
5. Zhang, W., Wang, C., Xie, F., Zhang, H.: Defect imaging curved surface based on flexible eddy current array sensor. *Measurement* **151**, 107280 (2020). <https://doi.org/10.1016/j.measurement>
6. Ma, Q., Gao, B., Tian, G., Yang, C., Xie, L., Chen, K.: High sensitivity flexible double square winding eddy current array for surface micro-defects inspection. *Sens. Actuator A* **309**, 111844 (2020). <https://doi.org/10.1016/j.sna.2020.111844>
7. Zhang, H., Ma, L., Xie, F.: A method of steel ball surface quality inspection based on flexible arrayed eddy current sensor. *Measurement* **144**, 192–202 (2019). <https://doi.org/10.1016/j.measurement>
8. Machado, M.A., Rosado, L., Pedrosa, N., Vostner, A., Miranda, R., Piedade, M., Santos, T.G.: Novel eddy current probes for pipes: Application in austenitic round-in-square profiles of ITER. *NDT E Int.* **87**, 111–118 (2017). <https://doi.org/10.1016/j.ndteint.2017.02.001>
9. Azad, A., Kim, N.: Design and optimization of an MFL coil sensor apparatus based on numerical survey. *Sensors* **19**, 4869 (2019). <https://doi.org/10.3390/s19224869>
10. Ramos, H.G., Ribeiro, A.L.: Present and future impact of magnetic sensors in NDE. *Procedia Eng.* **86**, 406–419 (2014). <https://doi.org/10.1016/j.proeng>
11. Gotoh, Y., Takahashi, N.: Proposal of detecting method of outer side crack by alternating flux leakage testing using 3-D nonlinear FEM. *IEEE Trans. Magn.* **42**, 1415–1418 (2006). <https://doi.org/10.1109/TMAG.2006.870939>
12. Gotoh, Y., Takahashi, N.: Study on problems in detecting plural cracks by alternating flux leakage testing using 3-D nonlinear Eddy

- current analysis. *IEEE Trans. Magn.* **39**, 1527–1530 (2003). <https://doi.org/10.1109/TMAG.2003.810219>
13. Kai, S., Chao, C., Yihua, K., Junjiang, L., Jilin, R.: Mechanism study of AC-MFL method using U-shape inducer. *Chin. J. Instrum.* **33**, 1980–1985 (2012). <https://doi.org/10.19650/j.cnki.cjsi.2012.09.009>
 14. Tsukada, K., Yoshioka, M., Kawasaki, Y., Kiwa, T.: Detection of back-side pit on a ferrous plate by magnetic flux leakage method with analyzing magnetic field vector. *NDT E Int.* **43**, 323–328 (2010). <https://doi.org/10.1016/j.ndteint.2010.01.004>
 15. Song, N., Haga, Y., Goda, T., Sakai, K., Kiwa, T., Tsukada, K.: Detecting internal defects of a steel plate by using low-frequency magnetic flux leakage method. In: 2017 IEEE Sensors Applications Symposium (SAS). IEEE, Glassboro, NJ, USA, pp. 1–6. (2017). <https://doi.org/10.1109/SAS.2017.7894069>
 16. Cherepov, S., Hesse, O., Mook, G., Pankratyev, S., Uchanin, V.: Optimisation of low frequency eddy current sensors using improved inductive coils and highly sensitive AMR and GMR sensor modules. In: Proceeding of the 13th IMEKO TC-4 International Symposium, pp. 568–576 (2004)
 17. Sophian, A., Tian, G.Y., Zairi, S.: Pulsed magnetic flux leakage techniques for crack detection and characterisation. *Sens. Actuator A* **125**, 186–191 (2006). <https://doi.org/10.1016/j.sna.2005.07.013>
 18. Wilson, J.W., Tian, G.Y.: Pulsed electromagnetic methods for defect detection and characterisation. *NDT E Int.* **40**, 275–283 (2007). <https://doi.org/10.1016/j.ndteint.2006.12.008>
 19. Wilson, J.W., Kaba, M., Tian, G.Y., Licciardi, S.: Feature extraction and integration for the quantification of PMFL data. *Nondestruct. Test. Eval.* **25**, 101–109 (2010). <https://doi.org/10.1080/10589750.802588010>
 20. Wang, P., Xiong, L., Sun, Y., Wang, H.: Tian G Features extraction of sensor array based PMFL technology for detection of rail cracks. *Measurement* **47**, 613–626 (2014). <https://doi.org/10.1016/j.measurement.2013.09.047>
 21. Altschuler, E., Pignotti, A.: Nonlinear model of flaw detection in steel pipes by magnetic flux leakage. *NDT E Int.* **28**, 35–40 (1995)
 22. Kundu, T., Bergamini, A., Christen, R.: A simple approach to the localization of flaws in large diameter steel cables. In: Paper presented at the Smart Nondestructive Evaluation and Health Monitoring of Structural and Biological Systems II, San Diego, California, USA (2003)
 23. Christen, R., Bergamini, A., Motavalli, M.: Three-dimensional localization of defects in stay cables using magnetic flux leakage methods. *J. Nondestruct. Eval.* **22**, 93–101 (2003). <https://doi.org/10.1023/B:JONE.0000010736.74285.b6>
 24. Lee, J., Choi, M., Jun, J., Kwon, S., Kim, J.-H., Kim, J., Le, M.: Nondestructive testing of train wheels using vertical magnetization and differential-type Hall-sensor array. *IEEE Trans. Instrum. Meas.* **61**, 2346–2353 (2012). <https://doi.org/10.1109/TIM.2012.2199190>
 25. Xie, S., Tian, M., Chen, H.-E., Zhao, Y., Wu, L., Chen, Z., Uchimoto, T., Takagi, T., Cheng, Z., Zhu, J., Li, Y., Sievert, J.: Evaluation of wall thinning defect in magnetic material based on PECT method under magnetic saturation. *Int. J. Appl. Electromagn. Mech.* **55**, 49–59 (2017). <https://doi.org/10.3233/jae-172257>
 26. Horai, S., Hirata, K., Niguchi, N., Kojima, F., Kobayashi, F., Nakamoto, H.: Flux-focusing eddy current sensor with magnetic saturation for detection of water pipe defects. *Int. J. Appl. Electromagn. Mech.* **52**, 1231–1236 (2016). <https://doi.org/10.3233/jae-162099>
 27. Deng, Z., Sun, Y., Kang, Y., Song, K., Wang, R.: A permeability-measuring magnetic flux leakage method for inner surface crack in thick-walled steel pipe. *J. Nondestruct. Eval.* **36**, 68 (2017). <https://doi.org/10.1007/s10921-017-0447-z>
 28. Song, K.: Study of signal mechanism based on combining magnetic flux leakage and eddy current testing. *J Mech Eng* **45**, 233–237 (2009). <https://doi.org/10.3901/JME.2009.07.233>
 29. Gotoh, Y., Sakurai, K., Takahashi, N.: Electromagnetic inspection method of outer side defect on small and thick steel tube using both AC and DC magnetic fields. *IEEE Trans. Magn.* **45**, 4467–4470 (2009). <https://doi.org/10.1109/tmag.2009.2024894>
 30. Yuji, G., Takahashi, N.: Evaluation of detecting method with AC and DC excitations of opposite-side defect in steel using 3-D nonlinear FEM taking the minor loop into account. *IEEE Trans. Magn.* **44**, 1622–1625 (2008). <https://doi.org/10.1109/tmag.2007.916486>
 31. Lou, W., Shen, C., Zhu, Z., Liu, Z., Shentu, F., Xu, W., Lang, T., Zhang, Y., Jing, Z., Peng, W.: Internal defect detection in ferromagnetic material equipment based on low-frequency electromagnetic technique in 20# steel plate. *IEEE Sens. J.* **18**, 6540–6546 (2018). <https://doi.org/10.1109/jssen.2018.2850977>
 32. Tian, G.Y., Wilson, J., Morozov, M.: Complementary electromagnetic non-destructive evaluation. *AIP Conf. Proc.* **1335**, 1256–1263 (2011). <https://doi.org/10.1063/1.3592078>

Publisher's Note Springer Nature remains neutral with regard to jurisdictional claims in published maps and institutional affiliations.